sustainability

MDPI

Article

Vulnerability Comparisons of Various Complex Urban Metro Networks Under Multiple Failure Scenarios

Yangyang Meng [1,2]

[1] The Hong Kong Polytechnic University Shenzhen Research Institute, Shenzhen 518000, China; yangyang.meng@polyu.edu.hk
[2] Department of Civil and Environmental Engineering, The Hong Kong Polytechnic University, Kowloon, Hong Kong SAR 999077, China

Abstract: Urban metro networks, characterized by their complex systems of interdependent components, are susceptible to a wide range of operational disturbances and threats. Such disruptions can cascade through the system, leading to service delays, operational inefficiencies, and substantial economic losses. Consequently, assessing and understanding network vulnerabilities have become crucial to ensuring resilient metro operations. While many studies focus on single-failure scenarios, comparative vulnerability analyses of various urban metro networks under multiple or simultaneous failures remain limited. To address this gap, our study introduces a comprehensive analytical framework comprising three key components: quantitative indices operating at both network and node levels, methodological approaches to assess the importance of network components (nodes, edges, and lines), and systematic protocols for evaluating vulnerabilities across multiple failure scenarios (stations, tunnels, lines, and areas). A comparative analysis of the Shenzhen Metro Network (SZMN) and the Zhengzhou Metro Network (ZZMN) validates the proposed methods. The results indicate that the SZMN demonstrates higher connectivity and accessibility than the ZZMN, despite a lower network density. Both networks are disassortative and heterogeneous, with edges connecting multiline transfer stations showing significantly higher edge betweenness centrality compared to those connecting general stations. In the SZMN, 6.63% of node failures and 4.74% of tunnel failures exceed a vulnerability threshold of 0.03, compared to 13.74% and 11.27% in the ZZMN. Failures across different lines and areas yield varying impacts on network performance and vulnerability. This study provides essential theoretical and practical insights, helping metro safety managers identify vulnerable points and strengthen the sustainable development of urban metro systems.

Keywords: complex metro networks; importance identification; vulnerability evaluation; multiple failure scenarios; comparative analysis

Citation: Meng, Y. Vulnerability Comparisons of Various Complex Urban Metro Networks Under Multiple Failure Scenarios. *Sustainability* **2024**, *16*, 9603. https://doi.org/10.3390/su16219603

Academic Editor: Caterina Malandri

Received: 26 September 2024
Revised: 28 October 2024
Accepted: 31 October 2024
Published: 4 November 2024

1. Introduction

The metro network is a fundamental pillar of modern urban transportation infrastructure, facilitating the daily mobility of millions of commuters [1]. Ensuring the reliable operation of these systems is essential to maintaining urban functionality and promoting metropolitan sustainability [2]. However, metro networks are highly complex systems, characterized by intricate interdependencies among their stations and lines, which make them inherently vulnerable to both intentional disruptions and random failures [3,4].

These systems face a range of threats during daily operations, with common disturbances stemming from both internal issues and external factors [5]. Internal issues include equipment malfunctions and human operational errors [6], such as vehicle breakdowns, mechanical and signal failures, power outages, and passenger-related incidents. External factors primarily refer to emergencies caused by environmental conditions and security concerns [6], such as natural disasters (e.g., severe rainstorms, earthquakes, snowstorms, heat waves) [7–9], terrorist attacks [10], and public health crises like the COVID-19 pandemic [11]. These disruptions and failures can manifest at multiple scales, from individual

station closures to network-wide interruptions, precipitating not only substantial operational delays and economic losses, but also posing significant risks to commuter safety and public health [12]. Given these far-reaching implications, a systematic analysis of metro network vulnerability under diverse failure scenarios is increasingly critical.

System vulnerability [13] refers to the likelihood that a system will experience degradation or failure when exposed to potential threats, disruptions, or adverse events, emphasizing the system's sensitivity to risk. In the context of metro networks, vulnerability denotes the extent of performance degradation following a disturbance or attack, with a focus on the changes in the system before and after the event [14,15]. Scholars have extensively investigated metro network vulnerability through diverse methodological approaches, including network modeling, critical node identification, vulnerability index development, scenario-based analysis, and empirical case studies. This body of research primarily encompasses five key domains: identifying influencing factors, consequence analysis, vulnerability assessment, recovery and resilience, and system optimization and improvement. Identifying influencing factors [16–19] aims to uncover the causes of disturbances from perspectives such as topology, redundancy, robustness, capacity, demand, and response and emergency mechanisms. Consequence analysis [20–22] evaluates the negative impacts of emergencies on the topology, operation, management, and economy of the metro network. Vulnerability assessments [23–25] typically involve quantitative modeling based on impact analysis, utilizing indicators such as failure probability, performance loss, and robustness to calculate system vulnerability. Recovery and resilience [25–28] studies focus on post-disturbance recovery strategies and system-wide changes throughout the entire process, informed by robustness and vulnerability analyses. Finally, optimization and improvement [29–31] concentrate on developing response measures to reduce system vulnerability and enhance inherent resilience in the face of future disturbances. The methodological framework spanning these five research domains encompasses theoretical analysis, mathematical modeling, scenario-based simulation, data-driven approaches, and various hybrid combinations thereof.

Failure scenarios play a critical role in studying the vulnerability of metro networks. Common failure scenarios are typically categorized into station closures, tunnel interruptions, line suspensions, and complete network collapses. The impact of disruptions on the metro network can vary significantly depending on their scale and extent [32]. Contemporary research in this field predominantly examines station-level failures by simulating disruptions according to predetermined protocols and then quantifying the resultant changes in network performance metrics and vulnerability indices. These simulations are commonly classified into random and intentional attacks [3,33,34], as well as static and dynamic conditions [20,24,35–37]. However, much of the existing research is centered on the vulnerability assessment of single-point failures, with limited attention given to multiple failure scenarios [5]. Real-world interruptions frequently involve cascading effects [7,17,38,39] or concurrent incidents [32], which can further complicate a system's vulnerability. Thus, examining metro network vulnerability under multiple concurrent failure scenarios is critical, as such analysis provides fundamental insights for enhancing the resilience and operational reliability of urban metro systems.

In summary, although existing research on metro network vulnerability has yielded significant insights, current studies predominantly examine system performance degradation under single-failure scenarios, with limited attention to the comparison of vulnerabilities in metro networks under multiple or simultaneous failure scenarios. To address this issue, this study presents a comprehensive analytical framework encompassing several key components. First, this study constructs a complex metro network model and proposes several measurement indicators to analyze the topological characteristics at both the network and station levels. Methods for evaluating the importance of nodes, edges, and lines are then introduced. The study also presents vulnerability measurement methods for station, tunnel, line, and area failures through simulation. Finally, to validate the proposed models, this study conducts an empirical analysis comparing two distinct cases: the Shenzhen

Metro, which faces frequent typhoon disruptions, and the Zhengzhou Metro, which has experienced severe rainstorm-induced failures. Through this comparative analysis—both horizontal across cities and vertical across different failure conditions—this study aims to identify critical vulnerabilities within complex metro networks. The insights gained from this research can contribute to the design of more resilient metro systems, enhance emergency planning, and mitigate losses in the face of unforeseen events.

The remainder of this paper is organized as follows: In Section 2, the methodology is proposed in detail. In Section 3, the study objects are described. In Section 4, the numerical analysis results are presented. Finally, in Section 5, the conclusions and future research are summarized.

2. Methods

Figure 1 presents the methodological framework of this study. Grounded in complex network theory and resilience principles, the analytical approach comprises three main components. First, this study constructs a complex network model of urban metro systems and analyzes their topological characteristics, followed by an evaluation of the relative importance of various network components. Subsequently, it simulates multi-level component failure scenarios and quantifies the resulting changes in vulnerability indices. Finally, the framework culminates in a comparative empirical analysis of the Shenzhen and Zhengzhou metro networks, examining vulnerability variations across different urban contexts and network components. The detailed methodological procedures for each analytical stage are elaborated in the following sections.

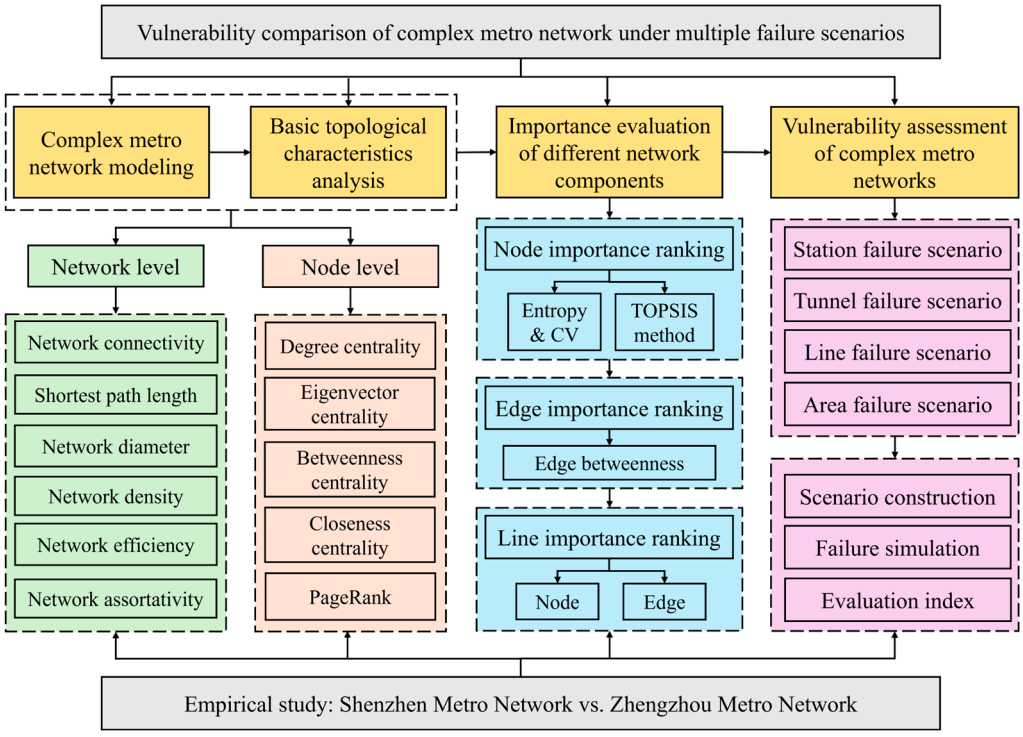

Figure 1. The overall research framework.

2.1. Complex Network Modeling and Basic Topological Indicators

In this study, the widely recognized Space L model is employed to construct the complex metro network $G = (V, E)$, where $N = \{v_i,\ i = 1, 2, \cdots, N\}$ represents the set of nodes, and $E = \{e_{ij},\ i, j = 1, 2, \cdots, N, i \neq j\}$ represents the set of edges. Each edge $e_{ij} = (v_i, v_j)$ corresponds to a connection between two adjacent nodes (i, j). In this metro network model, a node represents a station, and the edge between two adjacent nodes

corresponds to the tunnel connecting the stations. If stations (i, j) are adjacent, an associated adjacency matrix $A = [a_{ij}]$ is generated, where $a_{ij} = 1$; otherwise, $a_{ij} = 0$.

Based on complex network theory and graph theory, the topological characteristics of G can be quantified using various measures. In this study, a series of indicators are used to assess the network's basic topology. Beyond the most intuitive indicators, such as the number of network nodes N, the number of edges E, the number of lines L, the average degree $\overline{k} = \frac{1}{N}\sum_{i=1}^{N} k_i$ provides insights into the network's structure and scale. Network connectivity $\beta = \frac{E}{N}$ is employed to determine whether the network exhibits a loopy-type structure ($\beta > 1$) or a tree-type structure ($\beta < 1$). Additionally, the average shortest path length $APL = \frac{1}{N(N-1)}\sum_{i \neq j} d_{ij}$ and network diameter $D = maxd_{ij}$ are used to evaluate the network's connectivity and accessibility, while network density $\rho = \frac{2E}{N(N-1)}$ measures the degree of interconnectedness within the network.

Global efficiency θ is used to measure how efficiently information is exchanged across the entire network, defined as the average of the inverse shortest path lengths between all node pairs. A network with high global efficiency has a small average path length, indicating that information can be transmitted quickly between any pair of nodes. Local efficiency δ, on the other hand, assesses the efficiency of information transfer within the local neighborhoods of the network, evaluating how well the neighbors of a node communicate with each other in the event that the node is removed. This metric is crucial for gauging the network's robustness at a local level. Lastly, assortativity σ measures the similarity of connections in the graph concerning node degree, indicating whether nodes with similar degrees are more likely to be connected.

Node centralities [33,40], including degree centrality (DC), eigenvector centrality (EC), betweenness centrality (BC), closeness centrality (CC), and PageRank (PR), are commonly used to analyze the topological characteristics of nodes within complex networks. These centrality measures assess the role and significance of nodes from various perspectives and are often employed as fundamental indices for determining node importance.

2.2. Importance Evaluation of Complex Network Components

2.2.1. Node Importance Evaluation

By leveraging various node centrality measures, the Multi-Criteria Decision-Making (MCDM) method can be applied to comprehensively evaluate the importance of nodes. Common MCDM methods include the Analytic Hierarchy Process (AHP), the Weighted Sum Model (WSM), the Weighted Product Model (WPM), and the Technique for Order Preference by Similarity to Ideal Solution (TOPSIS), among others. Each method has its respective strengths and weaknesses. TOPSIS [40,41] is widely used to rank alternatives based on their distance from an ideal solution (the best possible score) and a nadir solution (the worst possible score). The optimal alternative is the one closest to the ideal and farthest from the nadir.

In this study, we utilize normalization to eliminate differences in dimensionality and magnitude. The improved TOPSIS method is used to evaluate the importance of nodes, with the weights obtained through the entropy weight (EW) method and the coefficient of variation (CV) method, which are combined using a preference coefficient. This process allows for the calculation of the comprehensive importance C_i of each node i within the network. The detailed steps of this procedure are shown in Algorithm 1.

Algorithm 1. Determination process of node importance

Input

The raw data of node centralities: $X_{nm} = \left[x_{ij}\right], i = 1, 2, \cdots, n; j = 1, 2, \cdots, m$, where n is the number of nodes, m is the number of evaluation indexes, and x_{ij} represents the jth index of the ith node.

Process

1. Normalize the decision matrix: $P_{ij} = \frac{x_{ij}}{\sum_{i=1}^{m} x_{ij}}$, where P_{ij} is the normalized value of x_{ij} and x_{ij} is the raw value.
2. Calculate the entropy for each criterion: $e_j = -k\sum_{i=1}^{m} P_{ij} ln\left(P_{ij}\right)$, where $k = 1/\ln(m)$, e_j is the entropy of criterion j, and P_{ij} is the normalized value.
3. Calculate the weights of each criterion: $w_j = \frac{1-e_j}{\sum_{i=1}^{n}(1-e_j)}$, where w_j is the weight of criterion j and e_j is the entropy of criterion j.
4. Calculate the variation coefficient $v_j = s_j/\overline{x_j}$, where s_j is the standard deviation and $\overline{x_j}$ is the mean.
5. Determine the combined weights based on the w_j and v_j: $W_j = \varphi w_{,j} + (1-\varphi)v_j$, where φ is the preference coefficient and $\varphi \in (0, 1)$.
6. Normalize the decision matrix: $x_{ij}^{*} = \frac{x_{ij} - \min\limits_{1\le k\le n}\left\{x_{kj}\right\}}{\max\limits_{1\le k\le n}\left\{x_{kj}\right\} - \min\limits_{1\le k\le n}\left\{x_{kj}\right\}}$, where m is the number of evaluation indexes and x_{ij} represents the jth index of the ith node.
7. Determine the ideal solutions Z_{imax} and nadir solutions Z_{imin} for each column Z_i: $Z = SW_j,\ z_{ij} = \left\{s_{ij}w_j\right\}$.
8. Calculate the Euclidean distance $D^{+} = \sqrt{\sum_{j=1}^{n}\left(Z_{imax} - z_{ij}\right)^2}$ and $D^{-} = \sqrt{\sum_{j=1}^{n}\left(z_{ij} - Z_{imin}\right)^2}$ of each alternative from the ideal and nadir solutions.
9. Rank alternatives based on their relative closeness $C = \frac{D^{+}}{D^{+}+D^{-}} \in [0, 1]$ to the ideal solution.

Output

The comprehensive importance C_i for each node i.

2.2.2. Edge Importance Evaluation

Edge Betweenness Centrality (EBC) is used to evaluate the importance of edges in complex networks. EBC is defined as the number of shortest paths between node pairs that pass through a given edge. A high EBC value indicates that the edge serves as a critical conduit for communication or flow between different regions of the network. For each pair of nodes s and t, the shortest paths are calculated, and the number of these paths that traverse the edge e is determined. The EBC is then calculated by summing these values for all node pairs. EBC can be computed using Equation (1), where V represents the set of nodes, $\sigma(s, t)$ denotes the total number of shortest paths between s and t, and $\sigma(s, t|e)$ is the number of those paths passing through edge e.

$$EBC_e = \sum_{s,t\in V} \frac{\sigma(s, t|e)}{\sigma(s, t)} \tag{1}$$

The EBC values of all edges can be ranked from highest to lowest. A larger EBC value signifies a more critical role of the edge within the network. Consequently, edge importance in the complex metro network can be effectively assessed using this method.

2.2.3. Line Importance Evaluation

A line in a metro network consists of the nodes it passes through and the connecting links between them. Therefore, the importance of a line can be weighted and measured based on the importance of its nodes and connecting edges. The calculation formula is provided in Equation (2). If line l contains n_l nodes, with adjacent nodes forming $n_l - 1$ edges, the importance I_{line} of line l is calculated as the sum of the node importance I_{node} and

the edge importance I_{edge}. The calculation is expressed in Equation (2), where C_i represents the importance of node i and EBC_e represents the importance of edge e.

$$I_{line} = \gamma I_{node} + \delta I_{edge} = \gamma \sum_{i=1}^{n_l} C_i + \delta \sum_{e=1}^{n_l-1} EBC_e \quad (2)$$

2.3. Vulnerability Assessment of Complex Metro Networks

The metro network may experience varying levels of disruption, ranging from micro to macro events, such as station closures, tunnel interruptions, line failures, or area-wide failures. When these scenarios occur, the network's performance degrades, making the system more vulnerable. In this context, we define the vulnerability of the metro network as the reduction in network connectivity and the extent of loss following an emergency. To assess the network performance Q, we employ network efficiency (NE) and the largest connected subgraph ratio (LCR) as indicators, as outlined in Equation (3). Network efficiency is a metric used to evaluate the effectiveness of information transmission or communication within the network, and it can be computed using Equation (4).

In a network, a connected component is a subset of nodes where a path exists between any two nodes within the subset and no node in the subset is connected to any node outside of it. The largest connected component (LCC) is the connected component containing the highest number of nodes [42]. Equation (5) defines the largest connected subgraph ratio (LCR) as the proportion of the largest connected subgraph to the total number of nodes in the network. The two parameters, α and β, in Equation (3) represent the weights corresponding to NE and LCR, respectively.

$$Q = \alpha NE + \beta LCR \quad (3)$$

$$NE = \frac{1}{N(N-1)} \sum_{i \neq j} \frac{1}{d_{ij}} \quad (4)$$

$$LCR = LCC/N \quad (5)$$

NE and LCR are commonly used to evaluate overall network connectivity. Higher values for these indicators signify better network connectivity. Additionally, these metrics are useful for assessing the network's robustness, where higher values indicate that the network can remain connected even when some nodes or edges are removed. In the event of an emergency, the network efficiency and the largest connected subgraph ratio decrease to NE' and LCR', respectively, and the system's new performance is denoted as Q' (as shown in Equation (8)). At this point, the vulnerability (V) of the system is represented by ΔQ, the degree of reduction in Q, which can be calculated using Equation (9).

$$NE' = \frac{1}{N'(N'-1)} \sum_{i \neq j} \frac{1}{d'_{ij}} \quad (6)$$

$$LCR' = LCC'/N \quad (7)$$

$$Q' = \alpha NE' + \beta LCR' \quad (8)$$

$$V = \Delta Q = Q - Q' \quad (9)$$

The various failure scenarios that may occur within the metro network are categorized below, and the corresponding vulnerability of the system under each failure type is evaluated.

2.3.1. Case 1: Node Failure

The most common failure scenario in a metro network is node failure, which in this study refers to the complete interruption of a station within the network, meaning the node can no longer transport passengers. The failure of general stations and transfer stations has different impacts on the network. To illustrate this, we use a simple network

shown in Figure 2a, consisting of 10 stations and 6 lines, including 7 general stations and 3 transfer stations. Stations *I*, *B*, and *J* serve as two-line, three-line, and four-line transfer stations, respectively.

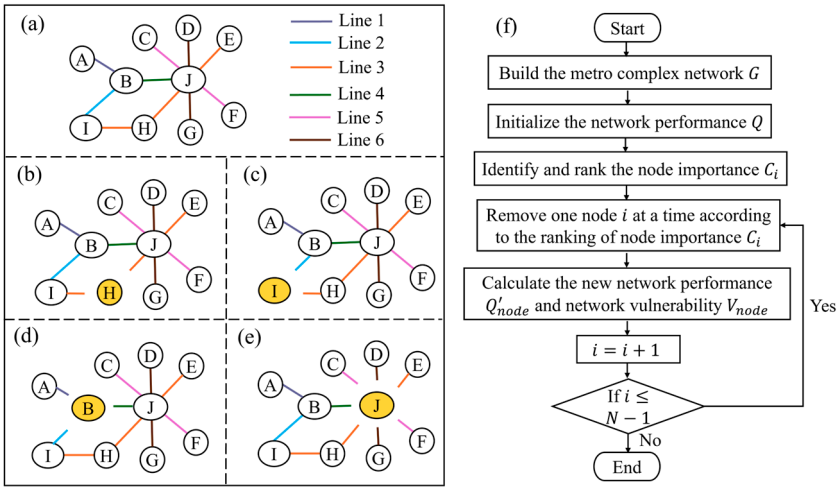

Figure 2. Simulation of node failure scenario: (**a**) the original network; (**b**) the failure of the general station *H*; (**c**) the failure of the two-line transfer station *I*; (**d**) the failure of three-line transfer station *B*; (**e**) the failure of the four-line transfer station *J*; (**f**) the simulation process.

Figure 2b–e depict the failure scenarios of different types of stations, with yellow indicating the stations that have failed. When the general station *H* fails, the connections *H-I* and *H-J* are severed, and a similar scenario occurs when the two-line transfer station *I* fails. However, when the three-line transfer station *B* fails, its adjacent stations *A*, *I*, and *J* become disconnected. In the case of the four-line transfer station *J* failing, all 7 of its connecting edges are disconnected from the network. For different types of station failures in the network, we simulate the impacts by sequentially removing the corresponding nodes from the network. First, we rank the importance C_i of all nodes from highest to lowest. Then, we remove one node at a time and calculate the network's performance, Q'_{node}, until all nodes have been assessed. Following this procedure, the network vulnerability V_{node} under the node failure scenario can be determined. The specific simulation process is illustrated in Figure 2f.

2.3.2. Case 2: Edge Failure

When the metro system is impacted by heavy rain, flooding, or similar events, water may enter the tunnels and disrupt the normal operation of the transit sections. In this case, edge failure in the metro network refers to the complete breakdown of a connected edge.

Figure 3a shows the original network. When the connecting edge between stations *B* and *I* fail, as depicted in Figure 3b,c, trains are unable to transport passengers along this section and must temporarily halt operations or alter the original operation plan. Like node failure, we simulate edge failure by sequentially removing the connected edges from the network. Figure 3d illustrates the specific simulation process. Based on the importance of all connected edges, the failure of a corresponding transit segment is simulated by removing one edge at a time. The network's performance, Q'_{edge}, is recalculated with each removal until all connected edges have been assessed. This allows us to evaluate the network's vulnerability, V_{edge}, under the edge failure scenario.

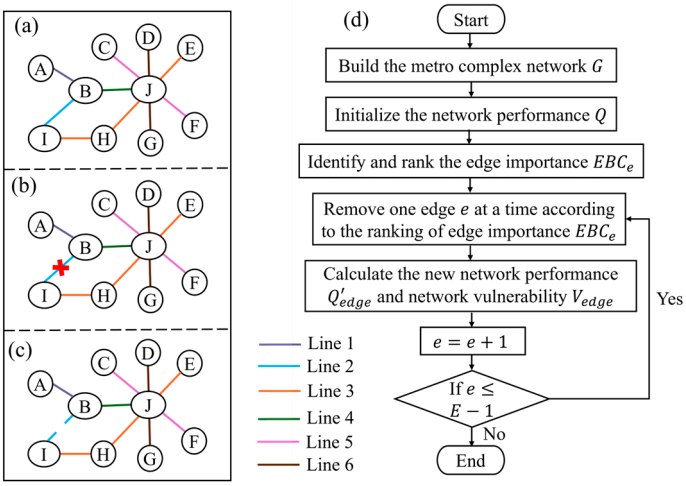

Figure 3. Simulation of edge failure scenario: (**a**) the original network; (**b**) the edge failure occurrence (the red color); (**c**) the state after failure: the interrupted edge; (**d**) the simulation process.

2.3.3. Case 3: Line Failure

Building on the potential node and edge failures caused by emergencies, when the disruption escalates, a chain reaction may result in the suspension of an entire line, leading to line failure. As shown in Figure 4b,c, when Line 3 fails, no trains can operate on the line, leading to the disconnection of the edges connecting stations *E*, *J*, *H*, and *I*. To simulate line failure, we remove all connecting edges between the nodes along the affected line in the network. The detailed simulation process is depicted in Figure 4d. This operation is performed on each line in the network, one at a time, and the performance of the updated network is calculated. In this way, the network vulnerability V_{line} under line failure conditions in the metro network can be assessed.

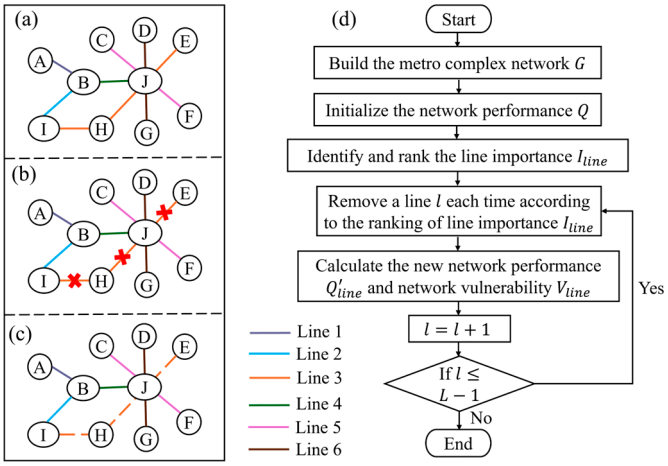

Figure 4. Simulation of line failure scenario: (**a**) the original network; (**b**) the line failure occurrence (the red color); (**c**) the state after failure: the interrupted line; (**d**) the simulation process.

2.3.4. Case 4: Area Failure

As the severity of an incident escalates, multiple connections and nodes within the metro network may be disrupted, leading to area failures. For instance, an extreme rainstorm may cause widespread flooding, rendering several stations and tunnels in a region inoperable. The light blue areas in Figure 5b represent flooded zones where stations *B*, *J*, *H*, and *I* are unable to operate normally. The closure of these stations directly prevents vehicle operations in the sections connecting them to adjacent stations, as illustrated in Figure 5c. To simulate such area failures, we remove all nodes within the affected area, as illustrated in Figure 5d. The connecting edges between these removed nodes become isolated, causing

the affected section to cease functioning. We then recalculate the network's performance, Q'_{area}, based on the changes. Finally, the network vulnerability V_{area} under the area failure scenario is determined.

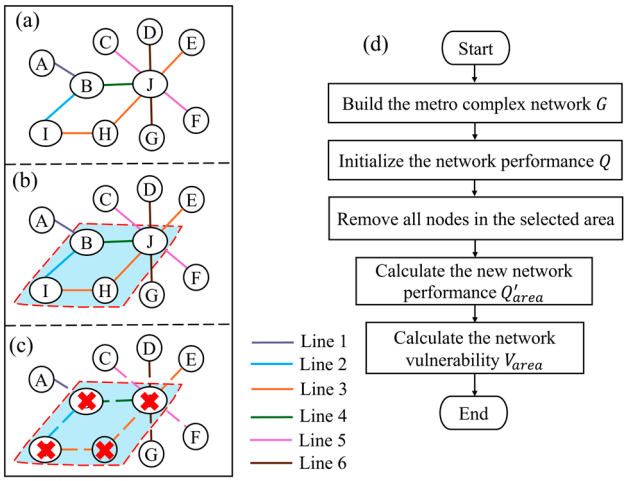

Figure 5. Simulation of area failure scenario: (**a**) the original network; (**b**) the flooding area (the blue parallelogram); (**c**) the interrupted stations (the red color); (**d**) the simulation process.

3. Study Objects

This study integrates relevant theories and real-world cases to select appropriate research objects. On 13 June 2017, heavy rain from Typhoon Merbok caused flooding at the entrance and exit of *Chegongmiao Station* on the Shenzhen Metro. Similarly, on 20 July 2021, the Zhengzhou Metro experienced extreme rainfall, resulting in water flooding the train tunnels and leading to a complete network shutdown. Given these metro network failure cases, this study selects the SZMN and ZZMN for case analysis, comparing their vulnerability under various failure scenarios.

At the end of 2017, the SZMN operated eight lines (L-1/2/3/4/5/7/9/11) with an operational length of 285.6 km. The network encompassed 166 stations, including one four-line transfer hub, two three-line transfer stations, and 25 two-line transfer stations. In comparison, by late 2021, the ZZMN consisted of seven lines (L-1/2/3/4/5/14/cj) covering 215.5 km, with 131 stations, of which 17 served as two-line transfer points. The schematic diagrams of SZMN and ZZMN are shown in Figure 6.

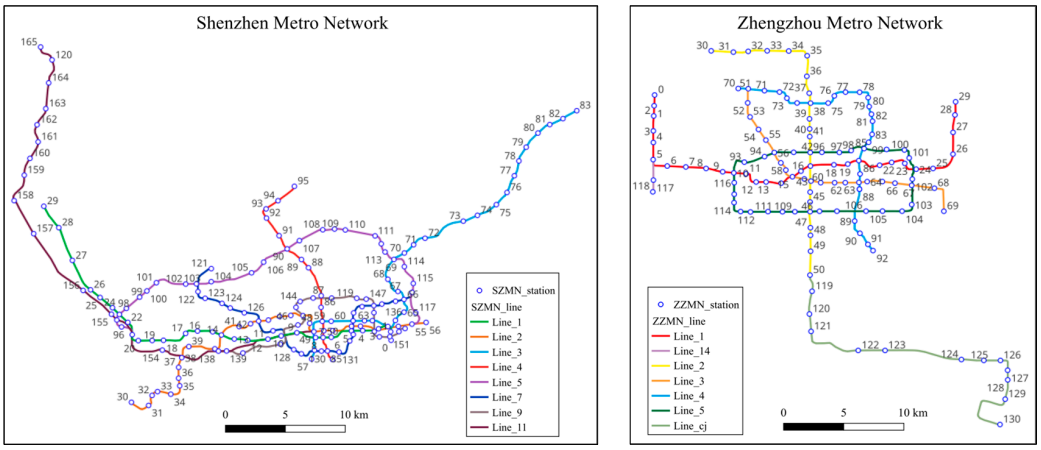

(**a**) (**b**)

Figure 6. Line diagram: (**a**) SZMN; (**b**) ZZMN.

4. Results

4.1. Basic Network Topological Characteristics

Based on the complex network models of the SZMN and ZZMN, along with relevant theories, their basic topological features can be quantitatively assessed, with the results presented in Table 1. In terms of the number of nodes, edges, and lines, the overall size of the SZMN is slightly larger than the ZZMN. The average degrees of the two networks are 2.289 and 2.168, respectively, showing minimal difference. Network connectivity can be understood by analyzing β, APL, and D. The network connectivity β of the SZMN is slightly higher than the ZZMN (1.145 vs. 1.084), while the APL of the SZMN is marginally lower than that of the ZZMN (11.64 vs. 11.77). The network diameter D of the SZMN is 43, which is 1.23 times that of the ZZMN. However, the ZZMN has a network density ρ of 0.0167, which is 1.20 times that of the SZMN. These values suggest that while the network density of the SZMN is slightly lower than that of the ZZMN, its connectivity and accessibility are higher.

In terms of network efficiency, SZMN demonstrates higher global efficiency θ than ZZMN (0.1323 vs. 0.1320), indicating that the information transmission speed between node pairs is faster in SZMN. The higher local efficiency δ of SZMN (0.003 vs. 0.000) suggests that local communication within the network is also more efficient, and the network exhibits greater robustness when a node is removed. Both networks have negative assortativity σ, indicating that they are disassortative and heterogeneous. Specifically, high-degree nodes tend to connect with low-degree nodes, and vice versa.

Figure 7 illustrates the geographical distribution of node centralities, revealing that the entire network is concentrated in the city's economically developed areas. The central areas are highlighted within two dashed boxes. Stations in these central areas exhibit higher proportions of CC and EC compared to other node centralities, whereas BC and CC are more prominent in other regions. In the SZMN network, *Chegongmiao Station*, a four-line transfer hub, demonstrates the highest DC, EC, BC and PR across the entire network. Conversely, *Futian Station*, a three-line transfer hub, exhibits the highest CC. Within the ZZMN network, all 16 two-line transfer stations, with the exception of *Nansihuan Station*, display the highest DC. *Zijingshan Station* leads in both EC and CC, while *Huanghelu Station* shows the highest BC. The largest PR value is observed at *Henan Orthopaedics Hospital Station*. On average, the four centralities, $\overline{DC}$, $\overline{EC}$, $\overline{BC}$, and $\overline{PR}$, are higher in ZZMN compared to SZMN, while $\overline{CC}$ is higher in SZMN than in ZZMN (0.0915 vs. 0.0903).

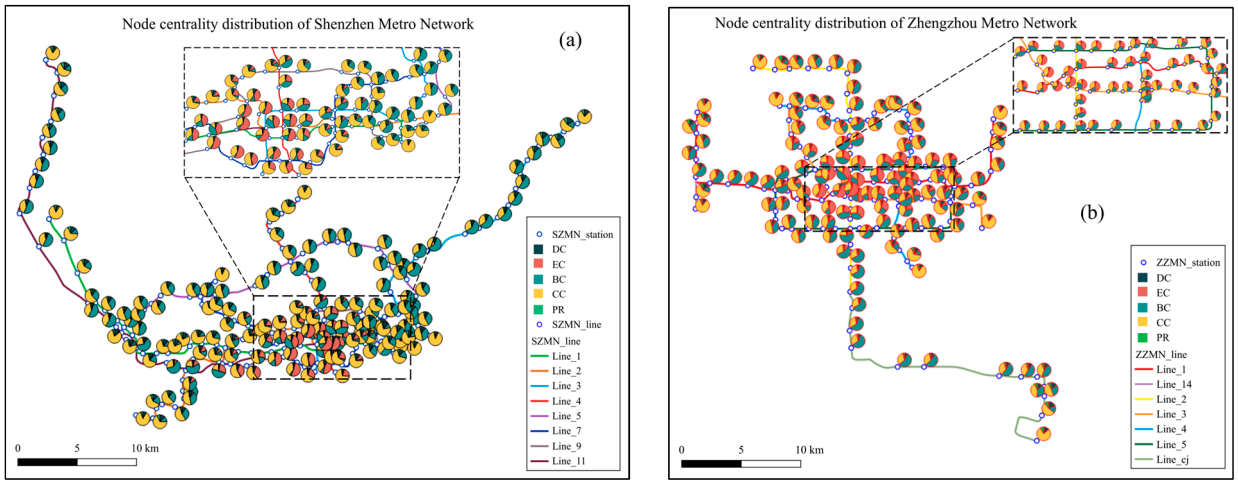

Figure 7. Geographical distribution of node centralities: (**a**) SZMN; (**b**) ZZMN.

Table 1. Basic topological characteristics of SZMN and ZZMN.

	N	E	L	$\bar{k}$	β	APL	D	ρ	δ	θ	σ
SZMN	166	190	8	2.289	1.145	11.64	43	0.0139	0.003	0.1323	−0.0431
ZZMN	131	142	7	2.168	1.084	11.77	35	0.0167	0.000	0.1320	−0.1055

4.2. Importance Ranking of Network Components

4.2.1. Node Importance Ranking

Using the node importance recognition method proposed in this study, we can determine the comprehensive importance values for all nodes in the two metro networks. The importance distributions of the 166 nodes in the SZMN and the 131 nodes in the ZZMN are depicted in Figure 8a,b. Overall, both networks contain a small number of highly important nodes. In the SZMN, 3.01% of the nodes have an importance value C greater than 0.5, compared to 4.58% in the ZZMN, while only 1.20% and 2.29% of the nodes in the SZMN and ZZMN, respectively, have C values exceeding 0.6. This indicates that most nodes hold low importance, highlighting the prominent network heterogeneity, where a few hub nodes play crucial roles. In the SZMN, *Chegongmiao Station* and *Futian Station* are the top two most important nodes, with importance values of 0.999 and 0.895, respectively. In the ZZMN, *Zijingshan Station*, *Dongdajie Station*, and *Huanghelu Station* are identified as the three most important nodes. The geographical distribution of node importance in the two networks is shown in Figure 8c,d. The larger the circle, the higher the node importance value C. Comparing the two networks, it is evident that the high C values in the SZMN are primarily concentrated in the southern part of the network, around *Chegongmiao* and *Convention & Exhibition Center*. In contrast, the high C values in the ZZMN are mainly located in the central part of the network, with a more uniform distribution of node importance compared to the SZMN.

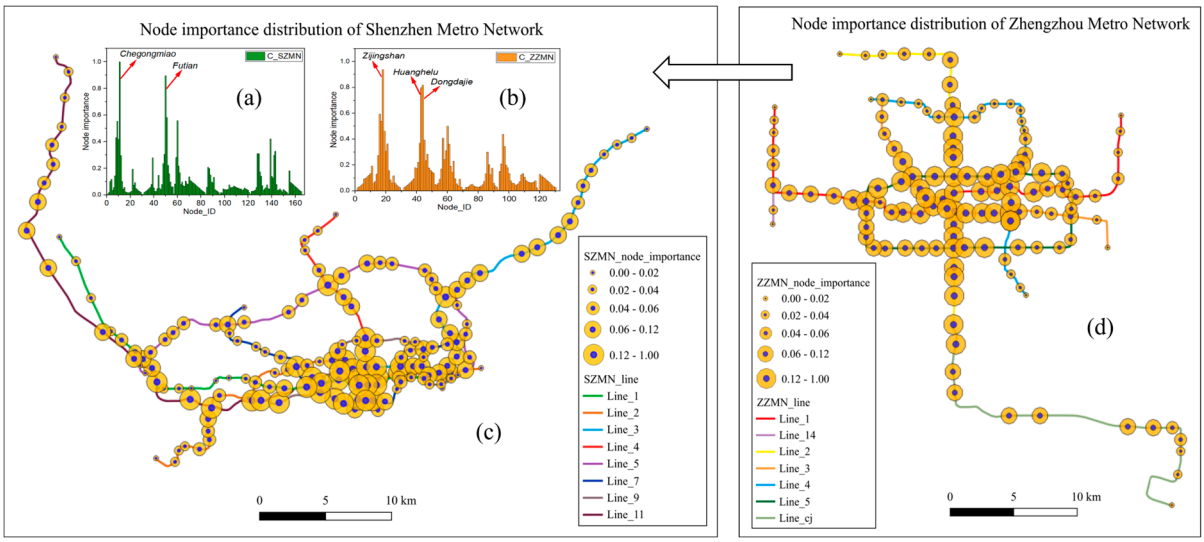

Figure 8. Statistical and geographical distribution of node importance in SZMN and ZZMN: (**a**) statistical distribution of node importance in SZMN; (**b**) statistical distribution of node importance in ZZMN; (**c**) geographical distribution of node importance in SZMN; (**d**) geographical distribution of node importance in ZZMN.

4.2.2. Edge Importance Ranking

By applying edge importance identification in the metro complex network, we can determine the EBC values and rankings of 190 edges in the SZMN and 142 edges in the ZZMN. The histograms of their frequency distributions are shown in Figure 9a,b. Overall, the frequency distribution of edge importance in the ZZMN follows a right-skewed normal

distribution, while the SZMN's distribution is closer to an exponential distribution. In terms of probability distribution, 53.16% of the edges in the SZMN have importance values in the range of [0, 0.05]. The proportion of edges with *EBC* values below 0.1 is 83.16%, while only 3.16% of the edges have *EBC* values greater than 0.20. In the ZZMN, 73.24% of the edges have *EBC* values less than 0.1, while only 4.93% of the edges have *EBC* values greater than 0.20. These findings indicate that in both networks, most edges demonstrate low importance ($EBC < 0.1$), with only a small fraction of edges holding high *EBC* values and occupying critical positions within the network's structure.

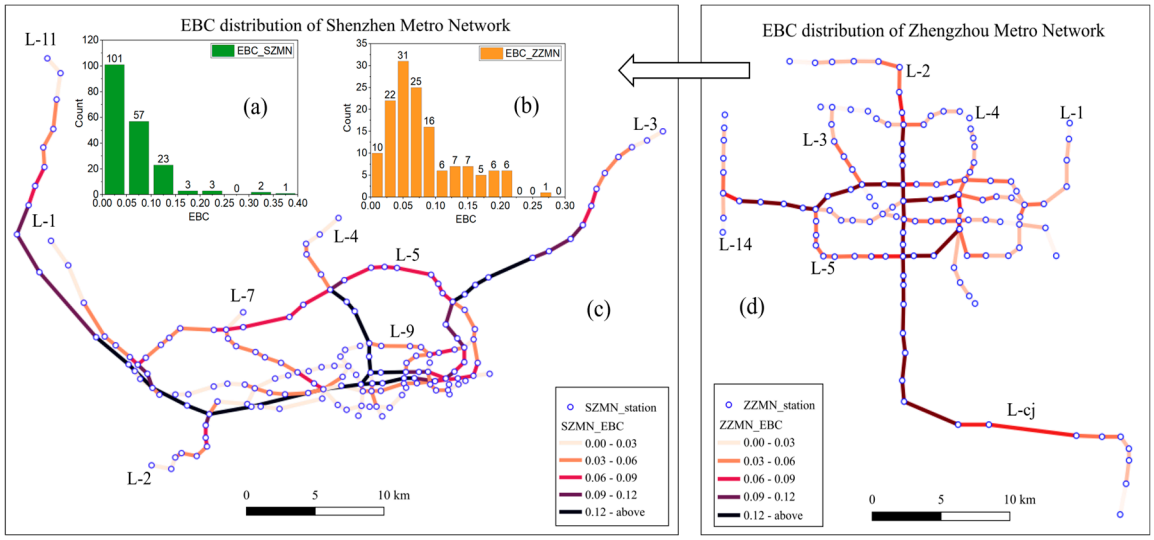

Figure 9. Frequency and geographical distribution of edge importance: (**a**,**c**) SZMN; (**b**,**d**) ZZMN.

Figure 9c,d visualize the geographical distribution of edge importance in the SZMN and ZZMN, respectively. In the SZMN, edges with high *EBC* values are predominantly concentrated along L-4 and L-11, with the edge connecting *Chegongmiao* and *Futian* having the highest *EBC* value (0.356). In the ZZMN, L-2 contains more edges with high *EBC* values, with the edge between *Zijingshan* and *Huanghelu* having an *EBC* of 0.261. Additionally, multi-line transfer stations in both networks exhibit higher *EBC* values compared to general stations.

4.2.3. Line Importance Ranking

Based on the line importance calculations, we obtain the importance values I_{line} for the 8 lines in SZMN and 7 lines in ZZMN. The detailed results are presented in Figure 10, showing significant variation in line importance across both networks. In SZMN, L-3 has the highest I_{line}, with a value of 7.12, while L-1, L-2, and L-11 all have I_{line} values exceeding 5. The average I_{line} for all lines in SZMN is 4.90, whereas in ZZMN it is slightly higher at 5.15. Notably, L-2 and L-5 in ZZMN have the highest I_{line} values, at 8.83 and 8.37, respectively, while L-14 has the lowest I_{line} value of only 0.17.

Comparing the I_{line} values of each line reveals that the status difference among lines in the SZMN is smaller than in the ZZMN. This may be attributed to the SZMN's earlier opening in 2004, resulting in a more balanced long-term development. In contrast, the ZZMN, which opened in 2013, is still in the early stages of rapid expansion, and the development planning for its different lines remains uneven. Understanding the ranking of line importance is valuable for assessing the status discrepancies between metro lines, especially in terms of planning, management, and operations. Furthermore, during emergencies that may cause service disruptions, the vulnerability and post-event resilience of various lines can differ significantly.

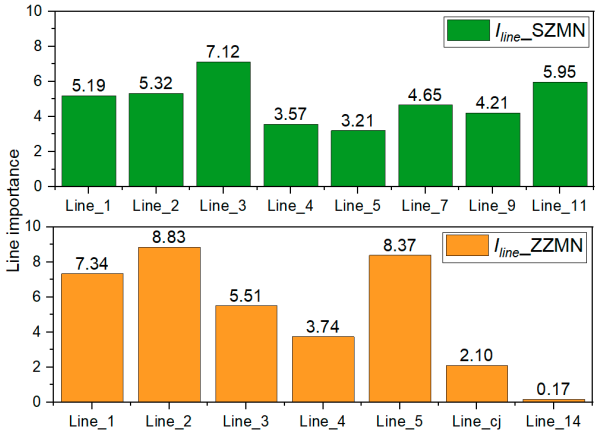

Figure 10. Line importance distribution of SZMN and ZZMN.

4.3. Vulnerability Assessment under Multiple Failure Cases

Based on the calculation of metro network vulnerability, the initial network efficiency for the SZMN and ZZMN is $NE^0_{SZ} = 0.1323$ and $NE^0_{ZZ} = 0.1320$, respectively. The initial largest connected subgraph ratios are both $LCR^0_{SZ} = LCR^0_{ZZ} = 1.00$. Since it is difficult to accurately determine the weights for these two indicators, we simplify Equation (3) by setting $\alpha = \beta = 0.5$. As a result, the initial network performance values are $Q^0_{SZ} = 0.5662$ and $Q^0_{ZZ} = 0.5660$. Next, we assess the vulnerability of each network under different failure scenarios.

4.3.1. Station Failure

The vulnerability results for the two metro networks under station failure are presented in Figure 11. The status of each node in the network determines the extent of the network's vulnerability when a failure occurs. Only a few node failures have a significant impact on network performance. In the SZMN, 6.63% of the nodes exhibit a vulnerability greater than 0.03 following failure, while 13.74% of the nodes in the ZZMN show such vulnerability. In previous studies [43], vulnerability was defined as the reduction in NE, leading to different results. In this study, we calculate vulnerability V based on both NE and LCR, and changes in these two metrics result in different vulnerability outcomes.

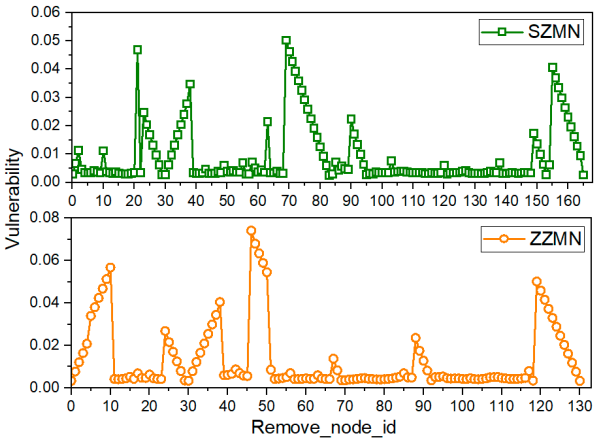

Figure 11. Vulnerability distribution under station failure.

In the SZMN, the node with the lowest NE following failure is *Chegongmiao Station* ($ID = 10$), with an NE value of 0.1159. However, the node with the lowest LCR is *Buji Station* ($ID = 69$), whose failure reduces the LCC from 166 to 151. Consequently, the scenario with the greatest vulnerability (0.0502) arises from the failure of *Buji Station*, where network performance drops to 0.5159. In the ZZMN, the failure of *Zijingshan Station*

($ID = 17$) results in the lowest NE value (0.1258), while the lowest LCC occurs with the failure of *Nanwulibao Station*, reducing the LCC to 114. As the change in LCR is greater than the change in NE, the failure of *Nanwulibao Station*, rather than *Zijingshan Station*, results in the highest performance degradation and the greatest vulnerability (0.0741). By comprehensively analyzing the geographical distribution of failed nodes in both networks, we find that the failure of *Buji Station* in the SZMN results in the disconnection of a portion of L-3 from the entire network. Similarly, the failure of *Nanwulibao Station* in the ZZMN causes the separation of part of L-2 and L-cj from the network. Both scenarios significantly disrupt the connectivity and accessibility of the respective networks, leading to the emergence of the most vulnerable failure scenarios.

4.3.2. Tunnel Failure

By applying the edge failure scenario analysis method proposed in this study, we can assess the system performance and vulnerability of metro networks under tunnel and section failures. Figure 12 presents the frequency distribution histogram of vulnerability V obtained from the edge failure simulations for the SZMN and ZZMN. In both networks, 80.53% and 76.76% of edge failure scenarios, respectively, have a vulnerability V less than 0.01, indicating that most tunnel failures result in relatively low vulnerability. Only 4.74% of edge failures in the SZMN and 11.27% in the ZZMN yield a network vulnerability greater than 0.03. Specifically, in the SZMN, the failure of the section linking *Buji Station* and *Muminawan Station* leads to the lowest network performance, with a drop to 0.5193, and the maximum vulnerability reaching 0.047. In the ZZMN, the failure of the edge between *Nanwulibao Station* and *Huazhai Station* results in the highest network vulnerability (0.0687). Notably, these two stations also rank as the top two with the highest vulnerability under the node failure scenario.

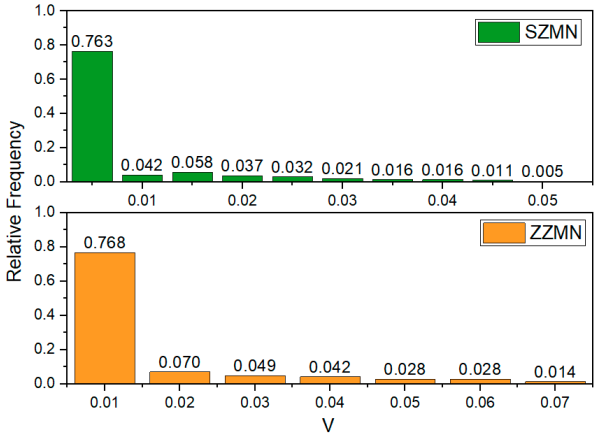

Figure 12. Frequency distribution histogram of V under tunnel failure.

4.3.3. Line Failure

When the metro network faces an emergency, such as a communication signal breakdown or power supply interruption, cascading failures can lead to the failure of an entire line. Using the line failure simulation method proposed in this study, we can assess the impacts of different line failures on the metro network, as shown in Figure 13. In the SZMN, the failure of L-1 results in the largest network vulnerability (0.0822), followed by L-3. In contrast, the failure of L-4 causes the smallest change in network performance, with the lowest vulnerability (0.0350). In the ZZMN, the failure of L-2 produces the highest network vulnerability (0.1311), while the failure of L-14 has the least impact, with a vulnerability of only 0.0090. The average network vulnerability of the SZMN's 8 lines under line failure is 0.0655, compared to 0.0863 for the ZZMN's lines.

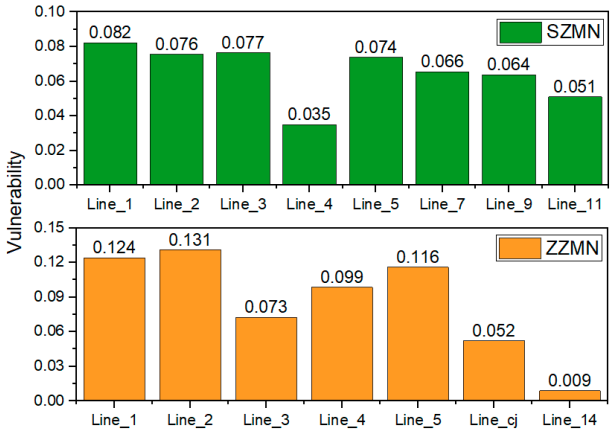

Figure 13. Vulnerability distribution under line failure.

4.3.4. Area Failure

For the failure of an area consisting of multiple stations and connecting edges, two regions, shown in Figure 14, are selected for simulation experiments. The selection is based on the basic topological characteristics of the two metro networks and actual passenger flow during operation. Figure 14a depicts failure area A in the SZMN, which includes *Chegongmiao*, *Futian*, *Shopping Park*, and *Xiangmihu*, as well as the links between adjacent stations. This area is chosen because it features a four-line transfer station, a three-line transfer station, a two-line transfer station, and a regular station, representing all station types in the SZMN and offering significant research value. In Figure 14b, failure area B in the ZZMN consists of *Zijingshan*, *Renminlu*, *Erqiguangchang*, *Xidajie*, *Dongdajie*, and the connecting edges between adjacent stations. The three vertices of the triangular region formed by these five stations are two-line transfer stations, underscoring this area's critical role in information transmission within the ZZMN.

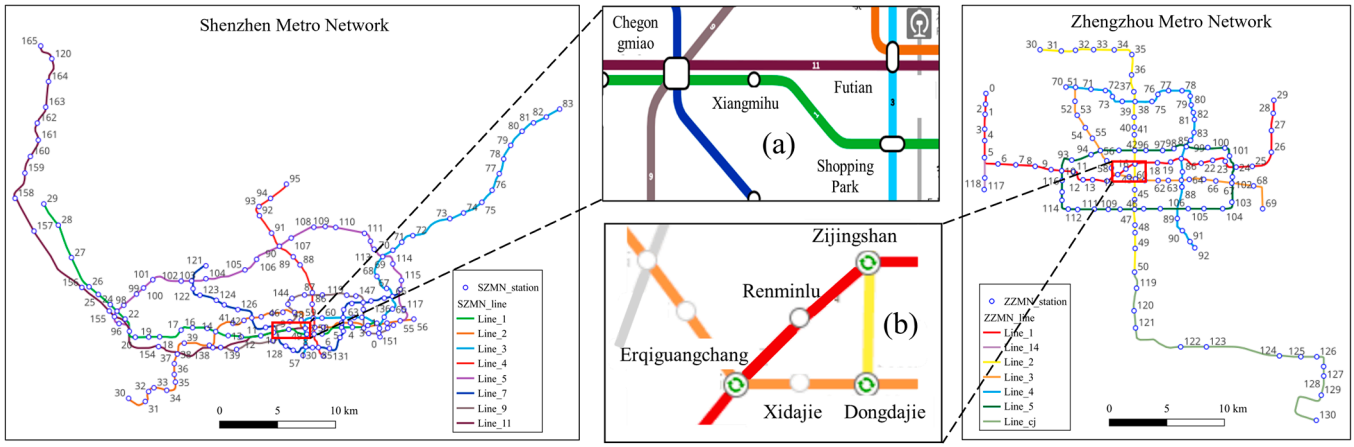

Figure 14. Area failure: (**a**) SZMN; (**b**) ZZMN.

Based on the area failure simulations, we can assess the changes in network performance and vulnerabilities for the two subnetworks, with detailed results presented in Table 2. In comparison to the initial network characteristics shown in Table 1, the number of connected edges in the SZMN is reduced by 15 following the failure of area A. *APL* increases from 11.64 to 14.99, and *D* rises from 43 to 46. Global network efficiency θ decreases by 15.65%, from 0.1323 to 0.1116. *LCC* decreases to 162, resulting in an *LCR* of 0.976. Consequently, network performance *Q* declines from 0.5662 to 0.5438, with a network vulnerability *V* of 0.0224. For the ZZMN, the number of connected edges decreases by nine after the failure of area B. *APL* increases from 11.77 to 13.16, and *D* rises from 35 to 40. *NE* drops to 0.1218, representing a 7.71% reduction from the initial condition. *LCR* is 0.962,

and the network vulnerability is 0.0242. Comparatively, the failure of area B has a slightly stronger impact on the ZZMN's performance than area A's failure has on the SZMN.

Table 2. Network characteristics of SZMN and ZZMN under area failure.

	N	*E*	*APL*	*D*	*θ*	*LCC*	*LCR*	$Q^{'}$	*V*
SZMN	162	175	14.99	46	0.1116	162	0.9759	0.5438	0.0224
ZZMN	126	131	13.16	40	0.1218	126	0.9618	0.5418	0.0242

4.3.5. Overall Comparison

Based on the four failure scenarios, we conducted a comparative analysis of the similarities and differences between the SZMN and ZZMN. A summary of results for both networks is presented in Table 3. Overall, the ZZMN exhibits higher overall vulnerability than the SZMN across node, edge, line, and specific area failure scenarios, with 13.74% of node failures and 11.27% of edge failures in the ZZMN resulting in vulnerabilities greater than 0.03. In comparison, the SZMN exhibits similar vulnerability levels in 6.63% of node failures and 4.74% of edge failures. Although the SZMN demonstrates lower average vulnerability than the ZZMN, it has a higher percentage of nodes with V > 0.03, indicating that the SZMN features a greater number of vulnerable nodes and edges. This suggests that if these critical components fail, the consequences for the SZMN could be more severe. Therefore, it is essential for metro management to enhance safety supervision of these components.

Table 3. Vulnerability changes under various failure scenarios.

Scenario	**Vulnerability (*V*)**		
	Index	**SZMN**	**ZZMN**
Node failure	V_avg	0.0091	0.0132
	$V \geq 0.03$	6.63%	4.74%
Edge failure	V_avg	0.0054	0.0088
	$V \geq 0.03$	13.74%	11.27%
Line failure	V_avg	0.0655	0.0863
Area failure	V	0.0224	0.0242

Empirical analysis of both metro networks reveals that disruptions to critical nodes generate more substantial impacts on network vulnerability compared to essential edge failures. Vulnerability impacts intensify as the scope of failure expands, with line-level disruptions demonstrating particularly significant effects. However, shorter lines—such as L-4 in the SZMN and L-14 in the ZZMN—contribute proportionally less to overall network robustness. The impact magnitude of area-based failures exhibits significant variation, primarily contingent upon the spatial distribution of the affected zones. Although typical areas in both networks were selected for simulation and analysis in this study, further examination of network performance under different regional failure scenarios is necessary. In general, node, edge, line, and area failures each have distinct effects on a given urban metro network, and different networks respond uniquely to identical failure scenarios. These dynamic interactions warrant further exploration from a dynamic perspective.

5. Conclusions and Future Works

This study proposes a method for identifying the importance of various network components (nodes, edges, and lines) based on complex metro network modeling and topological feature analysis. It also introduces vulnerability assessment methods for four failure scenarios: station, tunnel, line, and area. These methods are practically applied and comparatively analyzed in the SZMN and ZZMN networks, yielding the following key findings:

(1) Despite exhibiting lower network density, the SZMN demonstrates superior connectivity and accessibility metrics compared to the ZZMN. The higher global and local efficiency values found in the SZMN indicate enhanced information transmission capabilities and greater systemic robustness. Notably, both networks manifest disassortative mixing patterns and heterogeneous structural properties.

(2) Regarding network nodes, the values of $\overline{DC}$, $\overline{EC}$, $\overline{BC}$, and $\overline{PR}$ for the ZZMN are consistently higher than those of the SZMN, while $\overline{CC}$ of the SZMN exceeds that of the ZZMN. Both networks exhibit a small number of high-importance nodes, indicating prominent network heterogeneity, with a few hub nodes playing crucial roles in the network structure. Concerning network edges, the importance frequency distribution in the ZZMN approximates a right-skewed normal distribution, while that of the SZMN more closely resembles an exponential distribution. The proportion of edges with importance values greater than 0.20 is merely 3.16% in the SZMN, compared to 4.93% in the ZZMN. Multi-line transfer stations consistently demonstrate higher EBC values than general stations. Line importance varies significantly between the two networks, with the average I_{line} being 4.90 in the SZMN and 5.15 in the ZZMN. These disparities in network component criticality can be attributed to the distinctive infrastructure planning approaches and development trajectories adopted by each metro system.

(3) Network performance exhibits high sensitivity to disruptions among a small subset of critical nodes. In the SZMN, 6.63% of node failures result in a vulnerability greater than 0.03, while this proportion rises to 13.74% for the ZZMN. The failure of *Buji Station* has the most substantial impact on the SZMN's network performance, whereas *Nanwulibao Station's* failure induces the highest vulnerability in the ZZMN. Edge failures causing network vulnerability to exceed 0.03 are limited to 4.74% and 11.27% of cases in the SZMN and ZZMN, respectively. Network vulnerability peaks with the failure of Line-1 in the SZMN and Line-2 in the ZZMN. The impact of area A failure on the SZMN's vulnerability is marginally less severe than that of area B on ZZMN's performance. In general, different failure scenarios yield varying impacts on the performance and vulnerability of urban metro networks, underscoring the need to capture these dynamic changes.

Based on complex metro network topology, this study identifies the importance of various network components and evaluates network vulnerability under four failure scenarios across two urban metro systems. The research findings offer valuable insights for traffic planners and metro safety managers regarding the overall development of urban metro networks, the relative importance of the different components, and network performance changes under various failure scenarios. It can also assist in enhancing the safety supervision of vulnerable points during route operations and implementing effective measures during significant emergencies, ultimately improving the resilience and sustainability of metro network systems. However, this study has certain limitations. Future research endeavors should expand the analytical framework to incorporate key operational factors, specifically ridership patterns and environmental conditions, into vulnerability assessments. Moreover, subsequent investigations will focus on bridging theoretical frameworks with empirical scenarios to enhance the model's validity and practical applicability.

Funding: This research was funded by the National Natural Science Foundation of China (Grant No. 72304126).

Institutional Review Board Statement: Not applicable.

Informed Consent Statement: Not applicable.

Data Availability Statement: The original contributions presented in the study are included in the article, further inquiries can be directed to the corresponding author.

Conflicts of Interest: The author declares no conflicts of interest.

References

1. Yu, X.; Chen, Z.; Liu, F.; Zhu, H. How Urban Metro Networks Grow: From a Complex Network Perspective. *Tunn. Undergr. Space Technol.* **2023**, *131*, 104841. [CrossRef]
2. Shi, J.; Wen, S.; Zhao, X.; Wu, G. Sustainable Development of Urban Rail Transit Networks: A Vulnerability Perspective. *Sustainability* **2019**, *11*, 1335. [CrossRef]
3. Zhang, J.; Wang, S.; Wang, X. Comparison Analysis on Vulnerability of Metro Networks Based on Complex Network. *Physica A* **2018**, *496*, 72–78. [CrossRef]
4. Meng, Y.; Tian, X.; Li, Z.; Zhou, W.; Zhou, Z.; Zhong, M. Comparison Analysis on Complex Topological Network Models of Urban Rail Transit: A Case Study of Shenzhen Metro in China. *Physica A* **2020**, *559*, 125031. [CrossRef]
5. Sun, D.J.; Guan, S. Measuring Vulnerability of Urban Metro Network from Line Operation Perspective. *Transp. Res. Part A Policy Pract.* **2016**, *94*, 348–359. [CrossRef]
6. Chen, H.; Chen, B.; Zhang, L.; Li, H.X. Vulnerability Modeling, Assessment, and Improvement in Urban Metro Systems: A Probabilistic System Dynamics Approach. *Sustain. Cities Soc.* **2021**, *75*, 103329. [CrossRef]
7. Yang, Z.; Dong, X.; Guo, L. Scenario Inference Model of Urban Metro System Cascading Failure under Extreme Rainfall Conditions. *Reliab. Eng. Syst. Saf.* **2023**, *229*, 108888. [CrossRef]
8. Hu, J.; Wen, W.; Zhai, C.; Pei, S. A Comprehensive Review of Resilience of Urban Metro Systems: A Perspective from Earthquake Engineering. *Tunn. Undergr. Space Technol.* **2024**, *152*, 105920. [CrossRef]
9. Fraser, A.M.; Chester, M.V. Transit System Design and Vulnerability of Riders to Heat. *J. Transp. Health* **2017**, *4*, 216–225. [CrossRef]
10. Matsika, E.; O'Neill, C.; Battista, U.; Khosravi, M.; Laporte, A.D.S.; Munoz, E. Development of Risk Assessment Specifications for Analysing Terrorist Attacks Vulnerability on Metro and Light Rail Systems. *Transp. Res. Proc.* **2016**, *14*, 1345–1354. [CrossRef]
11. Zhang, Z.; Chai, H.; Guo, Z. Quantitative Resilience Assessment of the Network-Level Metro Rail Service's Responses to the COVID-19 Pandemic. *Sustain. Cities Soc.* **2023**, *89*, 104315. [CrossRef] [PubMed]
12. Huang, Z.; Loo, B.P.Y. Vulnerability Assessment of Urban Rail Transit in Face of Disruptions: A Framework and Some Lessons from Hong Kong. *Sustain. Cities Soc.* **2023**, *98*, 104858. [CrossRef]
13. Pan, S.; Yan, H.; He, J.; He, Z. Vulnerability and Resilience of Transportation Systems: A Recent Literature Review. *Physica A* **2021**, *581*, 126235. [CrossRef]
14. Gu, Y.; Fu, X.; Liu, Z.; Xu, X.; Chen, A. Performance of Transportation Network under Perturbations: Reliability, Vulnerability, and Resilience. *Transp. Res. E Logist. Transp. Rev.* **2020**, *133*, 101809. [CrossRef]
15. Lu, Q.-C.; Lin, S. Vulnerability Analysis of Urban Rail Transit Network within Multi-Modal Public Transport Networks. *Sustainability* **2019**, *11*, 2109. [CrossRef]
16. Liu, X.; Lei, Z.; Duan, Z. Assessing Metro Network Vulnerability with Turn-Back Operations: A Monte Carlo Method. *Physica A* **2024**, *646*, 129923. [CrossRef]
17. Lu, Q.-C.; Zhang, L.; Xu, P.-C.; Cui, X.; Li, J. Modeling Network Vulnerability of Urban Rail Transit under Cascading Failures: A Coupled Map Lattices Approach. *Reliab. Eng. Syst. Saf.* **2022**, *221*, 108320. [CrossRef]
18. Chen, H.; Shen, Q.; Feng, Z.; Liu, Y. Vulnerability Assessment in Urban Metro Systems Based on an Improved Cloud Model and a Bayesian Network. *Sustain. Cities Soc.* **2023**, *98*, 104823. [CrossRef]
19. Chen, H.; Zhang, L.; Ran, L. Vulnerability Modeling and Assessment in Urban Transit Systems Considering Disaster Chains: A Weighted Complex Network Approach. *Int. J. Disaster Risk Reduct.* **2021**, *54*, 102033. [CrossRef]
20. Zhang, Y.; Ayyub, B.M.; Saadat, Y.; Zhang, D.; Huang, H. A Double-Weighted Vulnerability Assessment Model for Metrorail Transit Networks and Its Application in Shanghai Metro. *Int. J. Crit. Infrastruct. Prot.* **2020**, *29*, 100358. [CrossRef]
21. Ma, F.; Liang, Y.; Yuen, K.F.; Sun, Q.; Zhu, Y.; Wang, Y.; Shi, W. Assessing the Vulnerability of Urban Rail Transit Network under Heavy Air Pollution: A Dynamic Vehicle Restriction Perspective. *Sustain. Cities Soc.* **2020**, *52*, 101851. [CrossRef]
22. Cats, O.; Jenelius, E. Beyond a Complete Failure: The Impact of Partial Capacity Degradation on Public Transport Network Vulnerability. *Transp. B Transp. Dyn.* **2018**, *6*, 77–96. [CrossRef]
23. Pan, S.; Ling, S.; Jia, N.; Liu, Y.; He, Z. On the Dynamic Vulnerability of an Urban Rail Transit System and the Impact of Human Mobility. *J. Transp. Geogr.* **2024**, *116*, 103850. [CrossRef]
24. Zhang, J.; Min, Q.; Zhou, Y.; Cheng, L. Vulnerability Assessments of Urban Rail Transit Networks Based on Extended Coupled Map Lattices with Evacuation Capability. *Reliab. Eng. Syst. Saf.* **2024**, *243*, 109826. [CrossRef]
25. Zhang, L.; Chen, T.; Liu, Z.; Yu, B.; Wang, Y. Analysis of Multi-Modal Public Transportation System Performance under Metro Disruptions: A Dynamic Resilience Assessment Framework. *Transp. Res. Part A Policy Pract.* **2024**, *183*, 104077. [CrossRef]
26. Zhang, D.; Du, F.; Huang, H.; Zhang, F.; Ayyub, B.M.; Beer, M. Resiliency Assessment of Urban Rail Transit Networks: Shanghai Metro as an Example. *Saf. Sci.* **2018**, *106*, 230–243. [CrossRef]
27. Ma, Z.; Yang, X.; Shang, W.; Wu, J.; Sun, H. Resilience Analysis of an Urban Rail Transit for the Passenger Travel Service. *Transp. Res. D Trans. Environ.* **2024**, *128*, 104085. [CrossRef]
28. Chen, C.; He, F.; Yu, R.; Wang, S.; Dai, Q. Resilience Assessment Model for Urban Public Transportation Systems Based on Structure and Function. *J. Saf. Sci. Resil.* **2023**, *4*, 380–388. [CrossRef]
29. Li, M.; Wang, H.; Wang, H. Resilience Assessment and Optimization for Urban Rail Transit Networks: A Case Study of Beijing Subway Network. *IEEE Access* **2019**, *7*, 71221–71234. [CrossRef]

30. Chen, J.; Liu, J.; Peng, Q.; Yin, Y. Strategies to Enhance the Resilience of an Urban Rail Transit Network. *Transp. Res. Rec.* **2022**, *2676*, 342–354. [CrossRef]
31. Zhang, L.; Xu, M.; Wang, S. Mitigating Vulnerability of a Multimodal Public Transit System for Sustainable Megacities: A Real-Time Operational Control Method. *Sustain. Cities Soc.* **2024**, *101*, 105142. [CrossRef]
32. Chen, C.; Wang, S.; Zhang, J.; Gu, X. Modeling the Vulnerability and Resilience of Interdependent Transportation Networks under Multiple Disruptions. *J. Infrastruct. Syst.* **2023**, *29*, 04022043. [CrossRef]
33. Yin, Y.; Huang, W.; Xie, A.; Li, H.; Gong, W.; Zhang, Y. Syncretic K-Shell Algorithm for Node Importance Identification and Invulnerability Evaluation of Urban Rail Transit Network. *Appl. Math. Model.* **2023**, *120*, 400–419. [CrossRef]
34. Sun, L.; Huang, Y.; Chen, Y.; Yao, L. Vulnerability Assessment of Urban Rail Transit Based on Multi-Static Weighted Method in Beijing, China. *Transp. Res. Part A Policy Pract.* **2018**, *108*, 12–24. [CrossRef]
35. Xiao, X.; Jia, L.; Wang, Y. Correlation between Heterogeneity and Vulnerability of Subway Networks Based on Passenger Flow. *J. Rai. Transp. Plan. Manag.* **2018**, *8*, 145–157. [CrossRef]
36. Zhao, J.; Liang, Q.; Guo, J.; Pu, K. Vulnerability Assessment and Evolution Analysis of Beijing's Urban Rail Transit Network. *Physica A* **2024**, *653*, 130078. [CrossRef]
37. Liu, B.; Zhu, G.; Li, X.; Sun, R. Vulnerability Assessment of the Urban Rail Transit Network Based on Travel Behavior Analysis. *IEEE Access* **2021**, *9*, 1407–1419. [CrossRef]
38. Ye, H.; Luo, X. Cascading Failure Analysis on Shanghai Metro Networks: An Improved Coupled Map Lattices Model Based on Graph Attention Networks. *Int. J. Environ. Res. Public Health* **2021**, *19*, 204. [CrossRef]
39. Chen, H.; Zhang, L.; Liu, Q.; Wang, H.; Dai, X. Simulation-Based Vulnerability Assessment in Transit Systems with Cascade Failures. *J. Clean. Prod.* **2021**, *295*, 126441. [CrossRef]
40. Meng, Y.; Tian, X.; Li, Z.; Zhou, W.; Zhou, Z.; Zhong, M. Exploring Node Importance Evolution of Weighted Complex Networks in Urban Rail Transit. *Physica A* **2020**, *558*, 124925. [CrossRef]
41. Liao, N.; Nawaz, M. An Indicator Model for Assessing Community Resilience to the COVID-19 Pandemic and Its Validation: A Case Study in Hong Kong. *J. Saf. Sci. Resil.* **2024**, *5*, 222–234. [CrossRef]
42. Zhang, J.; Wang, Z.; Wang, S.; Shao, W.; Zhao, X.; Liu, W. Vulnerability Assessments of Weighted Urban Rail Transit Networks with Integrated Coupled Map Lattices. *Reliab. Eng. Syst. Saf.* **2021**, *214*, 107707. [CrossRef]
43. Qi, Q.; Meng, Y.; Zhao, X.; Liu, J. Resilience Assessment of an Urban Metro Complex Network: A Case Study of the Zhengzhou Metro. *Sustainability* **2022**, *14*, 11555. [CrossRef]